ADVANCED MATERIALS

www.advmat.de

An Ultrastable Ionic Chemiresistor Skin with an Intrinsically Stretchable Polymer Electrolyte

Ming Liang Jin, Sangsik Park, Jong-Seon Kim, Sung Hyun Kwon, Shuye Zhang, Min Seok Yoo, Sungwoo Jang, Hyeong-Jun Koh, Soo-Yeon Cho, So Young Kim, Chi Won Ahn, Kilwon Cho, Seung Geol Lee, Do Hwan Kim, and Hee-Tae Jung**

Ultrastable sensing characteristics of the ionic chemiresistor skin (ICS) that is designed by using an intrinsically stretchable thermoplastic polyurethane electrolyte as a volatile organic compound (VOC) sensing channel are described. The hierarchically assembled polymer electrolyte film is observed to be very uniform, transparent, and intrinsically stretchable. Systematic experimental and theoretical studies also reveal that artificial ions are evenly distributed in polyurethane matrix without microscale phase separation, which is essential for implementing high reliability of the ICS devices. The ICS displays highly sensitive and stable sensing of representative VOCs (including toluene, hexane, propanal, ethanol, and acetone) that are found in the exhaled breath of lung cancer patients. In particular, the sensor is found to be fully operational even after being subjected to long-term storage or harsh environmental conditions (relative humidity of 85% or temperature of 100 °C) or severe mechanical deformation (bending to a radius of curvature of 1 mm, or stretching strain of 100%), which can be an effective method to realize a human-adaptive and skin-attachable biosensor platform for daily use and early diagnosis.

Chemiresistor sensors for the early diagnosis of human diseases and detection of chemicals in the environment have attracted considerable attention in recent years due to their simple, inexpensive, rapid, portable, power efficient, and highly sensitive sensing properties.[1–4] Various sensing materials for chemiresistors have been explored, including metal oxides,[5–7] monolayer-capped metal particles,[8–11] metal nanowire,[12–14] conducting polymers,[15] carbon nanotubes,[16,17] and 2D materials.[18–20] For example, metal oxides such as SnO_2, ZnO, TiO_2, WO_3, In_2O_3, Fe_2O_3, and CuO have been widely studied as channel materials due to their high sensitivity to specific gas molecules, easy production, and cost-effectiveness.[21–26] Also, 2D materials, including graphene, transition metal dichalcogenides (TMDs), boron/carbon nitride, and black phosphorus (BP), have been considered to be potential chemical sensing materials because of their unique electrical and surface properties.[27–32] In particular, their large surface-to-volume ratio leads to a high density of adsorption sites, easily tunable bandgap when changing the number of layers, and various active sites (e.g., at vacancies, edges, basal planes, and defects) for realizing highly selective molecular adsorption.[33–35] However, despite the intensive efforts in this field, the development of channel materials with long-term stability (mechanical and chemical robustness) as well as high selectivity and sensitivity is still very limited to be realized for practical use of flexible chemiresistor sensor.

Recently, ionic liquids (ILs) have been suggested as a promising chemiresistor sensor material due to their several significant advantages. First of all, ILs are endowed with negligible vapor pressure, wide potential windows, and nonflammability

Dr. M. L. Jin, Dr. J.-S. Kim, Dr. S. Jang, H.-J. Koh, S.-Y. Cho, Prof. H.-T. Jung
Department of Chemical and Biomolecular Engineering (BK-21 Plus)
Korea Advanced Institute of Science and Technology (KAIST)
Daejeon 305-701, South Korea
E-mail: heetae@kaist.ac.kr

Dr. M. L. Jin, Dr. J.-S. Kim, Dr. S. Jang, H.-J. Koh, S.-Y. Cho, Prof. H.-T. Jung
KAIST Institute for the NanoCentury
Daejeon 305-701, South Korea

Dr. M. L. Jin, Dr. C. W. Ahn
Department of Nano-Structured Materials Research
National NanoFab Center (NNFC)
291 Daehak-ro, Yuseong-gu, Daejeon 305-338, South Korea

The ORCID identification number(s) for the author(s) of this article can be found under https://doi.org/10.1002/adma.201706851.

DOI: 10.1002/adma.201706851

S. Park, S. Y. Kim, Prof. D. H. Kim
Department of Chemical Engineering
Hanyang University
Seoul 04763, South Korea
E-mail: dhkim76@hanyang.ac.kr

S. Park, M. S. Yoo, Prof. K. Cho
Department of Chemical Engineering
Pohang University of Science and Technology
Pohang 37673, South Korea

S. H. Kwon, Prof. S. G. Lee
Department of Organic Material Science and Engineering
Pusan National University
Busan 46241, South Koreaa

Dr. S. Zhang
State Key Laboratory of Advanced Welding and Jointing
Harbin Institute of Technology
Harbin 150001, China

and have proved to be stable sensing materials.[36,37] Also, unlike chemiresistor sensors based on metal oxides, IL-based chemiresistor sensors can be operated at room temperature due to their sustainably high conductivity levels.[38,39] In addition, it is relatively easy to derive efficient IL pairs because there are many types of both cationic and anionic ILs with a wide range of chemical structures, which can potentially form different interactions with different gases and hence bind target gases with high selectivity.[40,41] However, IL-based devices show a critical limitation: poor stability due to liquid flow in the external environment, especially when the device as a result becomes mechanically deformed. This fluidic nature of ILs that generates signal fluctuations in response to mechanical stress.[42,43] Although solid-state polymer electrolytes that are formed by combining polymer matrix with ILs can be used to enhance the stability of the devices, many polymers are poorly miscible with ILs, particularly at the concentrations of ILs high enough for realizing a high conductivity.[44,45] It is therefore very important in sensor research to carry out rational designs of solid-state polymer electrolyte films so that they exhibit good mechanical and environmental stability as well as high conductivity during operation. Moreover, in addition to being made mechanically stable, films used for wearable devices also need to be stretchable. Skin-attachable electronics with high stretchability enables excellent interaction with the human body to monitor signals in ways that bypass limitations of traditional technologies.[46,47] In fact, all components of wearable devices need to be intrinsically stretchable and mechanically robust.[48,49]

Herein, we provide the first report of an ultrastable, highly sensitive, and deformable chemiresistor sensor skin using an ion channel formed by a stretchable thermoplastic polyurethane matrix, namely ionic thermoplastic polyurethane (i-TPU), as a solid-state polymer electrolyte. The i-TPU electrolyte was formed as a result of the noncovalent interaction, between 1-ethyl-3-methylimidazolium bis(trifluoromethylsulfonyl)-imide ($[EMIM]^+[TFSI]^-$) and TPU matrix, to form that cation–anion pairs were then loaded into the TPU matrix. Our ionic chemiresistor skin (ICS) with the i-TPU electrolyte displayed an ultrastable response (accurate base line recovery and low signal noise) and negative electronic signal to five volatile organic compounds (VOCs), specifically toluene, hexane, propanal, ethanol, and acetone. Different molecular interactions made between i-TPU and the different VOCs resulted in different levels of ion conductivity for the ILs embedded in the TPU matrix. The limit of detection (LOD) of the ICS device for toluene gas was 1 ppm with a sensitivity level of 1.6%. More importantly, the sensor was found to be fully operational even after being subjected to harsh environmental conditions (relative humidity (RH) of 85% or temperature of 100 °C) or severe mechanical deformation (bending to a radius of curvature of 1 mm or a stretching strain of 100%). We believe that this ultrastable, highly sensitive, and stretchable ICS has potential to serve as a human-adaptive, skin-attachable biosensor platform, capable of detecting chemically diverse analytes for early diagnosis of disease and for environmental protection purposes.

Figure 1a shows a schematic illustration of the fabrication ICS with stretchable i-TPU electrolyte as a VOC sensing channel. The details of the method used to fabricate the i-TPU material and of the process used to fabricate the device are described in the Experimental Section. The i-TPU electrolyte film was formed as a result of the noncovalent interaction of ($[EMIM]^+[TFSI]^-$) cation–anion pairs with TPU matrix, which made the ion pairs of ILs were loaded into the TPU matrix. The ILs, which served as a plasticizer, in the TPU matrix partially enabled the intercalation of IL ions between hard segments and binding of IL ions to soft or hard segments of the TPU. Furthermore, most of the ions were expected to become located in the nanoscale free volume of the TPU film, which has been shown to be formed by soft and hard segments.[50] Support for this concept was derived from the results of various characterizations shown in **Figure 2**, and discussed below. In order to assess the capabilities of the ICS devices in detecting the various VOCs, the devices were loaded into the in-house-fabricated customized VOC reaction chamber that included multiarray systems and that was connected to a gas control system and to a multiplexing data-acquisition module as shown in Figure 1b. The simultaneously generated resistance sensing signals from separated channels were stably and reproducibly recorded with a constant bias supplement. During the measurements, the flow rates of N_2 (reference gas) and VOCs into the chamber were maintained at 400 sccm. Each VOC was injected into the chamber over the course of 5 min, followed by 20 min of N_2 purging before the next VOC injection. The temperature of the sensing chamber for the thermal stability test was controlled by using a mounted heating plate. Detailed information about the gas control system is provided in Figure S1 in the Supporting Information.

The hierarchically assembled i-TPU electrolyte films were observed to be very uniform, transparent, and intrinsically stretchable (see Figure 2a). The i-TPU electrolyte films, regardless of IL concentration, were also shown using UV–vis spectroscopy to be highly transparent, specifically ≈90% transparent to 550 nm wavelength light (Figure S2, Supporting Information). In general, stretchable electronic devices contain various materials with different Young's modulus (E) values, from fluids (Pa–kPa) to elastic materials (MPa) to hard and brittle materials (GPa).[51] To be mechanically compatible with biological tissues for skin-attachable electronics, all components of a chemiresistor should display a low modulus (≈MPa) with high flexibility and high stretchability.[52] In order to explore the mechanical properties of i-TPU electrolyte films, their stress–strain curves were obtained. For all of the i-TPU films, i.e., with the various IL concentrations, the stress–strain curves showed linear trends without saturation, and no specific deformation behavior was observed even up to 800% strain, as shown in Figure 2b. In particular, the i-TPU film with 60 wt% IL showed an E of ≈3.6 MPa, comparable to that of a typical PDMS film (E ≈1–2 MPa). Based on this result, we expect the i-TPU film to be a very effective solid-state polymer electrolyte and to contribute to the ability to produce a well-defined stretchable ICS (see Table S1 in the Supporting Information for details).

In order to understand the internal microstructure of the i-TPU electrolyte film, Raman spectroscopy, Differential Scanning Calorimeter (DSC), and the X-ray diffraction (XRD) analyses were carried out. The Raman spectra revealed the distributions in the TPU matrix of the ILs with various concentrations. The average of the Raman spectra taken from each of the various samples (i.e., having different concentrations of the IL in the

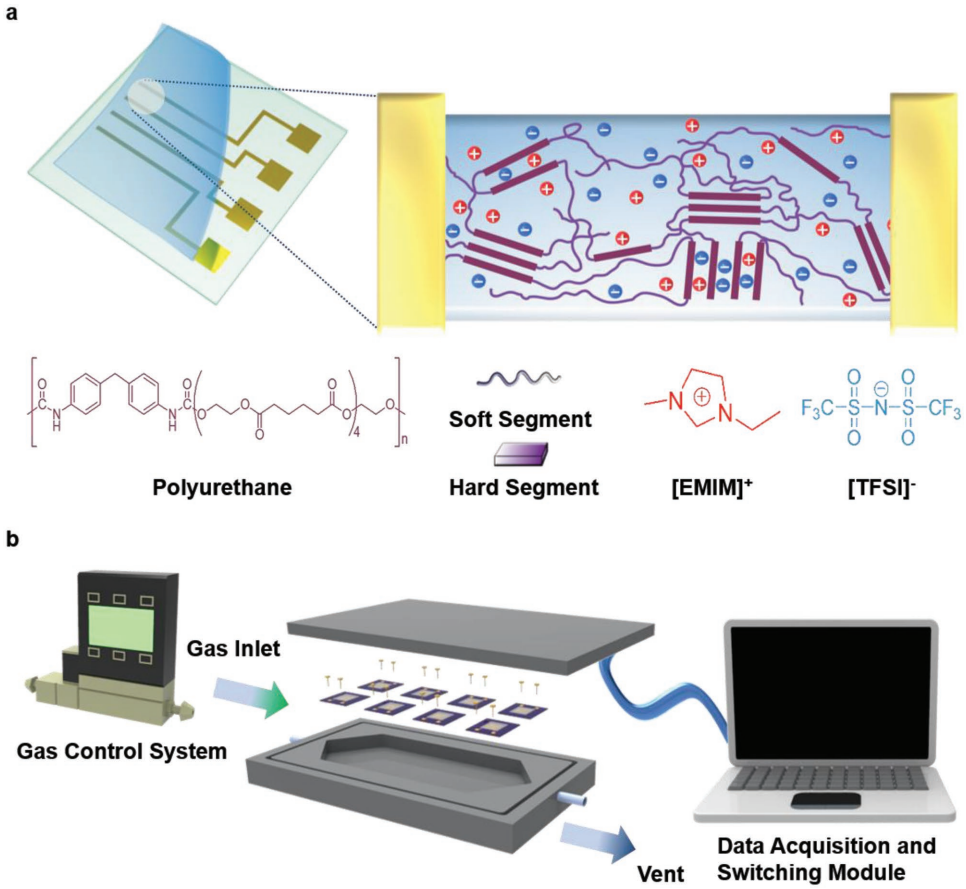

Figure 1. Schematic description of the individual ICS and VOC reaction chamber that we assembled and used. a) Schematic illustrations of the individual ICS based on a TPU polymer matrix with the ionic liquid consisting of $[EMIM]^+$ and $[TFSI]^-$ (top). Detailed schematic structures of TPU (and the soft and hard segments forming blocks along the TPU polymer backbone) (purple), $[EMIM]^+$ (red), and $[TFSI]^-$ (blue) (bottom). b) Schematic diagram of the customized VOC reaction chamber connected with a gas control system and data acquisition module.

TPU matrix) showed the signature peaks of $[EMIM]^+[TFSI]^-$ and TPU (see Figure S3 and Table S2, Supporting Information).[53] The Raman maps (5 μm × 5 μm) show the intensity ratio of anion to TPU and cation to TPU at different composition of ILs, respectively (Figure 2c). The Raman intensities of anion and cation of ILs are obtained from intensity of SO_2 symmetric stretching of anion centered at 1146 cm^{-1}, and intensity of antisymmetric stretching, C–C stretching, $(N)CH_2$ stretching, and $CH_3(N)CN$ stretching of cation centered at 1433 cm^{-1}, respectively, while that of TPU is achieved from intensity of polyester(C=O) and urethane amide (C=O) of TPU centered at 1740 cm^{-1}. It should be noted that the Raman peaks corresponding to the IL anions and cations were observed in the whole scanned region with a uniform intensity ratio, and that the intensity ratio was found to increase as the relative amount of IL in the sample was increased. This results showed that $[EMIM]^+[TFSI]^-$ was evenly distributed in the TPU matrix without microscale phase separation regardless of how much IL was in the TPU matrix. In addition, DSC curves (see Figure S4, Supporting Information) show the inner microstructure change of TPU upon various amount of IL. The neat TPU exhibits the glass transition temperature (T_g) of –34.8 °C and endothermic melting of crystalline domains (T_m) of 165.2 °C. With increasing the concentrations of IL into TPU, the T_g and T_m show a shift toward lower temperature, which is due to the plasticizer effect of IL.[54] The detail on plasticizing effect on IL will be discussed below. Figure 2d shows the XRD profile of a neat TPU film and i-TPU films with different concentrations of $[EMIM]^+[TFSI]^-$ to further elucidate the internal structure change upon addition ILs into TPU. The neat TPU shows a weak and broad crystalline XRD reflections at $2\theta \approx 19.79°$ (d-spacing = 4.48 Å), which is resulted from the hard segment crystalline domains in the TPU.[55] After incorporating ILs into the TPU, the peak positions at 19.79° are slightly decreased as increasing ionic concentration (20 wt%: 19.63°, 40 wt%: 19.28°, and 60 wt%: 19.16°). Obviously, these observations indicated that some ions went inside the hard segment and partially plasticized the crystalline domains of the TPU matrix. This interpretation in turn would further suggest that the ion pairs were mainly located in the free volume derived from the soft and hard segments of the i-TPU and were partially intercalated between the hard segments.

To further understand the molecular interaction between the TPU chain and the ion pairs, a density functional theory (DFT) calculation was performed (Figure 2e). The partially positive charged atoms in the TPU were selected for the possible binding sites for $[TFSI]^-$, and the partially negative charged

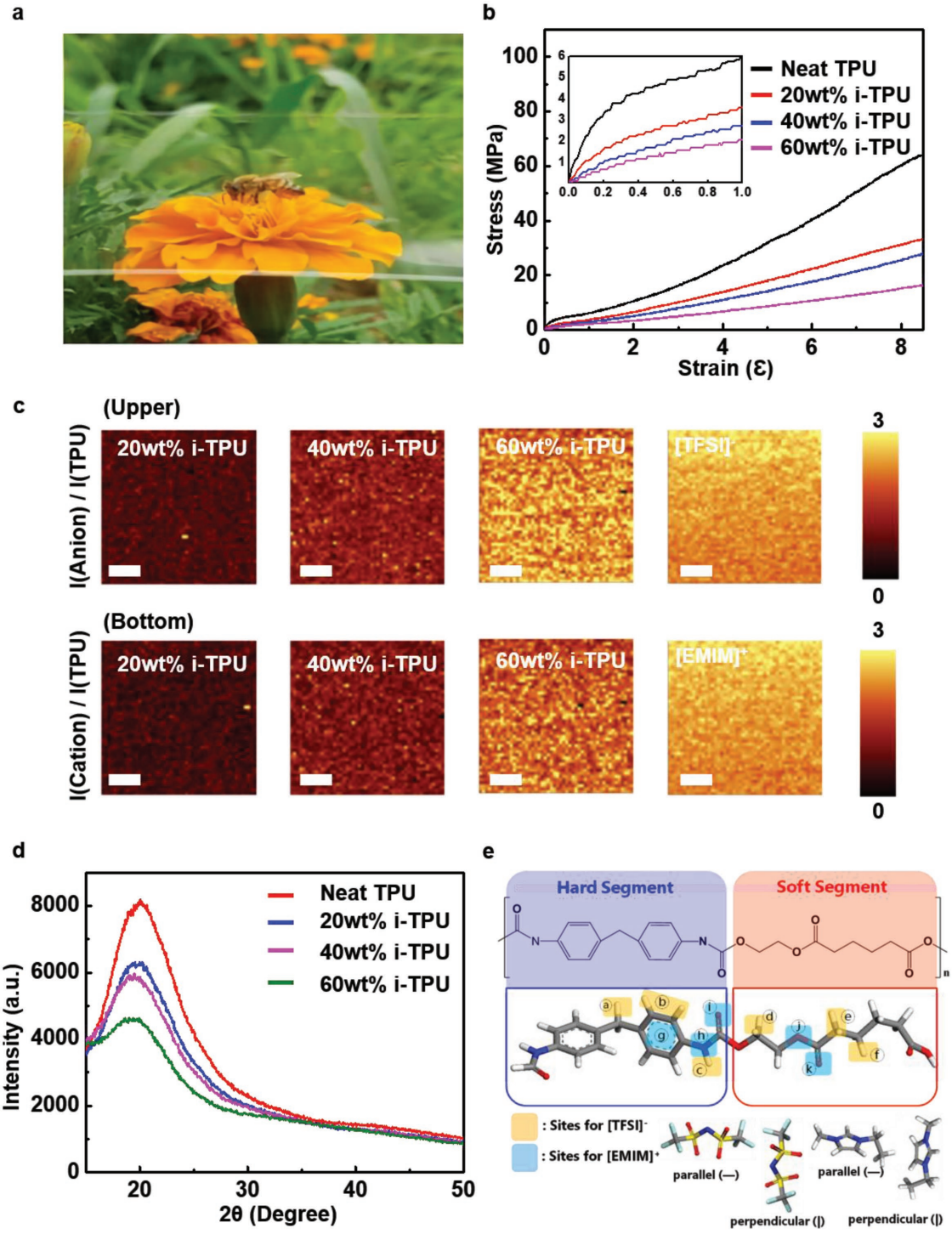

Figure 2. Basic characterizations of the synthesized i-TPU sensing material. a) Photographic of the highly transparent i-TPU material with 60 wt% IL. b) Stress–strain curves for i-TPU materials with various concentrations of the ionic liquid. c) Raman intensity ratio maps for various compositions: maps of I(anion)/I(TPU) and I(cation)/I(TPU) are shown in the top and bottom rows, respectively. Scale bar: 1 µm. d) XRD patterns of i-TPU materials with different concentrations of ionic liquid. e) DFT calculations for the possible binding sites of $[EMIM]^+[TFSI]^-$ ion pairs with two configurations on the TPU chain.

atoms in the TPU were selected for the possible binding sites for $[EMIM]^+$. The two different configurations, i.e., parallel (—) and perpendicular (|) binding positions on the TPU for each ion, were also considered. However, we did not consider the sites at the end of the TPU chain as possible binding sites of the IL to avoid the end effect of the TPU. The average binding energies of $[TFSI]^-$ for the hard and soft segments of the TPU were calculated using DFT to be –0.511 and –0.457 eV,

respectively, while the average binding energies of $[EMIM]^+$ for these segment were calculated to be –0.021 and –0.006 eV, respectively (see Figure 2e and Table S3, Supporting Information). Thus, $[TFSI]^-$ was determined to contribute more to the molecular interactions with the TPU chain than was $[EMIM]^+$. This result might have been due to the strong electronegative components such as F, O, and N in $[TFSI]^-$. By carrying out a Mulliken electronic population analysis, it was verified that the electronegative atoms in $[TFSI]^-$ can split a large amount of partial charge with the neighboring C and S atoms, hence providing a strong interaction with the TPU as shown in Table S4 in the Supporting Information. Therefore, ILs could plasticize over the hard and soft segments of the TPU. Note that this strong interaction nature of IL enfeebles the intermolecular interaction between TPU and IL so as to enhance the segmental motion of TPU. Also, the higher binding energies of $[TFSI]^-$ with TPU indicated an especially important role for $[TFSI]^-$ in partially plasticizing the crystalline domains. The computational details of the DFT simulations are described in the Experimental Section.

The dynamic sensing responses of the ICS devices were investigated by using the home-made gas-sensing channel with multiarray systems (see above and Experimental Section). **Figure 3**a shows the resistive response ($\Delta R/R_b$) of the ICS (60 wt% i-TPU electrolytes) with sequential exposure to five VOCs each at a concentration of 1000 ppm at room temperature. R_b and ΔR denote the baseline resistance of the sensors measured in a pure N_2 stream and the change in resistance resulting from the exposure to the VOCs, respectively. The VOCs in this work were selected as representatives of the main categories of compounds (aromatic compounds, aliphatic hydro carbons, aldehydes, alcohols, and ketones) found in the exhaled breath of lung cancer patients.[56] We firstly assessed the sensing performance of the VOC as a function of the concentration of the IL in the TPU matrix (Figure S6, Supporting Information). Dynamic sensing behavior of ICS shows that the sensing responses are very stable. In particular, the devices with 60 wt% i-TPU display highly stable performance with the accurate baseline recovery, due to the trade-off between electric conductivity and mechanical stability. It is important to note that an IL-based sensing device without TPU was not stable to fully and rapidly recover the baseline signal after ceasing flow of the VOC and instead flowing N_2 gas, due to the fluidic property of the ILs. All of these VOCs yielded electrical signals indicative of stable and negative responses in the ICS, which were related to the change in the ionic conductivity of the i-TPU electrolyte as a result of exposure of the sensor to the VOC, but the shapes of these signals differed for the different VOCs. Furthermore, from the resistance behaviors in Figure 3a, we extracted the sensitivity of the sensor for each VOCs, where the sensitivity was defined as the steady state value of the sensing response ($\Delta R/R_b$) after exposure to the target gas at room temperature. This ICS is greatest sensitive to toluene (≈10%), and the sensitivities are not much different for hexane (6.18%), propanal (6.12%), and ethanol (7.62%). On the other hand, the sensitivity to acetone gas is relatively as low as 1.91%. The response time $\tau_{90\%}$ (time it takes to reach the 90% value of the minimum resistance level) was extracted from Figure 3a, and shows not much difference with toluene (13 s), hexane (16 s), propanal (15 s), ethanol (18 s), and acetone (20 s). In addition, Figure S7 in the Supporting Information exhibits the similar gas sensitivity regardless of the i-TPU

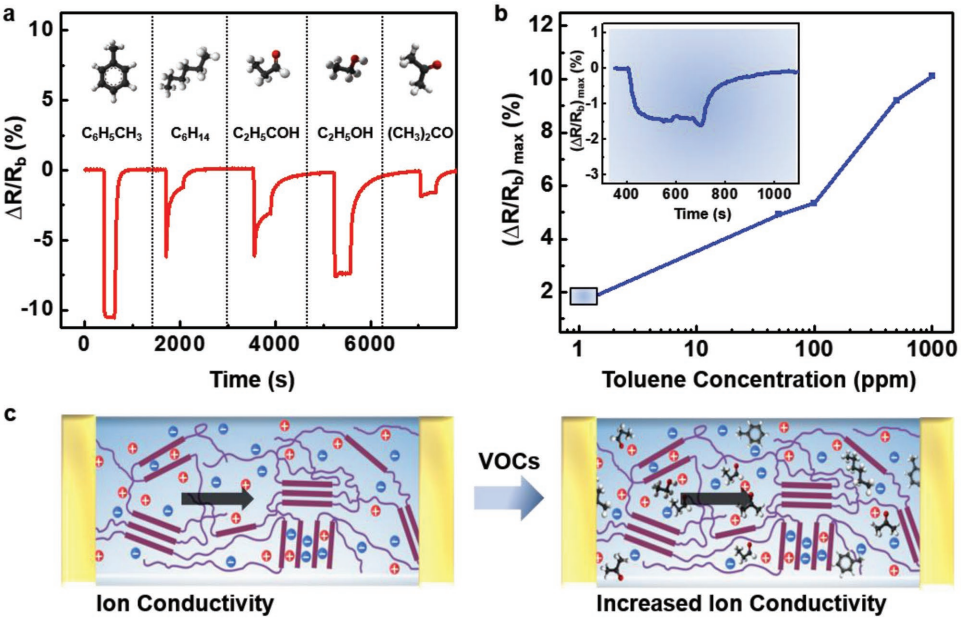

Figure 3. Dynamic sensing behavior of the ICS to VOCs, and the sensing mechanism of the ICS. a) Response of the ICS to each target VOC (toluene, hexane, propanal, ethanol, and acetone) at a concentration of 1000 ppm, showing the ultrastable and negative gas-sensing properties of the sensor. b) The ICS response to toluene gas in the range 1 to 1000 ppm. Inset shows the response of the ICS to the toluene gas at a concentration of 1 ppm. c) Schematic illustration of a proposed mechanism of the sensing of target VOCs by the i-TPU sensing channel. The VOCs would according to this mechanism affect the ionic conductivity of ILs confined by the soft and hard segments of the TPU matrix, resulting in a negative resistance change of the sensing channel.

channel thickness, but some thickness effect on the response time.

To determine the LOD of the ICS, the sensing responses to toluene at various concentrations from 1 to 1000 ppm were measured as shown in Figure 3b. As a whole, the change in resistance tended to increase as the concentration of the injected toluene gas was increased. Interestingly, the ICS showed an obvious change in resistance at a concentration of toluene as low as 1 ppm (inset of the Figure 3b), indicative of a very low LOD for this sensor (inset of the Figure 3b).

A possible mechanism for how the ICS sensed the various VOCs is illustrated in Figure 3c. The negative electrical responses to all of the VOCs indicated that in each case, the resistance of the device decreased as a result of the interaction between the IL in the i-TPU channel and the VOC, and hence the ionic conductivity of the $[EMIM]^+[TFSI]^-$ channel was enhanced.[57] The change in the ionic conductivity for i-TPU after exposure to VOCs (1000 ppm of toluene, hexane, and acetone, respectively) was analyzed in more detail using electrochemical impedance spectroscopy (Figures S5 and S8, Supporting Information). As shown in Figure S8 in the Supporting Information, $\Delta\sigma/\sigma_i$ increased for each type of VOCs. Furthermore, the amount of increase for each VOCs corresponded to that of $\Delta R/R_b$ shown in Figure 3a. The effects of IL viscosity and diffusivity on ionic conductivity can be explained using Equations (1) and (2).[57] According to Seddon,[58] the viscosity of a mixture of an IL and dissolved VOC gas as a function of the concentration of the dissolved VOC gas can be written as

$$\eta = \eta_s \exp\left(-\frac{\chi_{cs}}{a}\right) \quad (1)$$

where η_s and η are the viscosities of the pure $[EMIM]^+[TFSI]^-$ and VOC-dissolved IL at 20 °C, χ_{cs} is the mole fraction of the VOC, and a is a constant for the specific IL. The relation between viscosity and diffusivity can be expressed from the Stokes–Einstein equation

$$D = \frac{k_B T}{6\pi\eta r} \quad (2)$$

where D is the diffusion coefficient of the charged ions, k is the Boltzmann constant, T is the absolute temperature, and η is the viscosity of the IL.[59] Dissolution of a VOC into an IL would tend to result in a decrease in the viscosity of the IL with this decrease inducing an increase in the IL diffusivity and hence also ion conductivity.[60,61] Therefore, the marked difference between the shapes of the electrical signals we observed for the different VOCs was attributed to the different degrees of change in $[EMIM]^+[TFSI]^-$ ionic conductivity caused by the different VOCs (Figure 3c).

In order to investigate the stability of the ICS device, we measured its response ($\Delta R/R_b$) to toluene gas (1000 ppm) after storing it under ambient, high humidity, or high-temperature robust conditions for specified periods of time (**Figure 4**). In ambient conditions, the magnitude of the response of the device to the toluene gas changed negligibly over the course of a month (Figure 4a), indicative of the high long-term stability of the ICS.

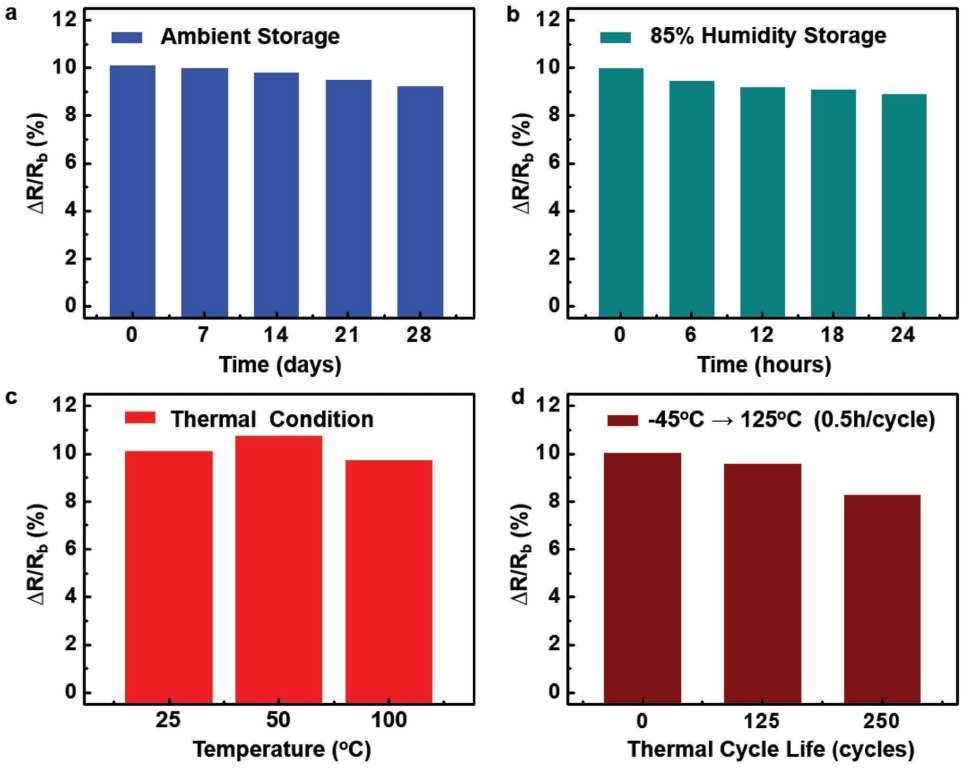

Figure 4. The ability of the ICS to sense the VOC toluene at 1000 ppm was found to be ultrastable in a variety of environments. a) The resistive response ($\Delta R/R_b$) of the ICS stored under ambient conditions for a month. b) Response of the ICS stored at 85% relative humidity for 24 h. c) Responses of ICS stored at various temperatures up to 100 °C. d) Responses of the ICS subjected to various numbers of thermal cycles with the temperature raised from °45 to 125 °C in 0.5 h in each cycle.

Moreover, as shown in Figure 4b, the magnitude of the response of our ICS to the toluene under the harsh relative humidity of 85% was both very stable for 24 h and similar to the magnitude of the response at ambient conditions. The sensing response at different humidity (30%, 60%, and 85%) levels after storage the devices for 24 h is described in Figure S9 in the Supporting Information. Both the long-term stability and environmental robustness of the sensor were attributed to the water and air resistance of the i-TPU electrolyte. The stability of the sensor performance to specifically high RH conditions was attributed to the relatively poor miscibility of $[EMIM]^+[TFSI]^-$ with water, with this poor miscibility resulting from $[EMIM]^+[TFSI]^-$ being more hydrophobic than most conventional ionic liquid.[62] In addition, the high hydrophobicity and low O_2 permittivity of the TPU matrix[63] also benefited the durability of our solid-state i-TPU electrolyte in the presence of water and oxygen, and hence the resistance of the ICS to the environment and the stability of its performance.

The effect of temperature on the long-term stability of the chemiresistor-type VOC sensor is another important factor to consider, since not only may the surrounding conditions for measuring sensor characteristics differ from the user's external thermal environment, but also the response of the device can be severely affected by a change in the gas permittivity to the i-TPU channel. Thus, the magnitude of the response of our ICS to the 1000 ppm toluene gas was measured under various temperature conditions, including 25, 50, and even the extremely high value of 100 °C (Figure 4c and Figure S10, Supporting Information).

The magnitudes of response at the different temperatures differed a bit, but the device was able to bear the high temperature (100 °C) and still show high sensitivity. We also examined the effect of thermal aging on the sensing performance by carrying out a thermal cycling test. As shown in Figure 4d, no significant change in the capability of the ICS device to sense the toluene gas was observed as a result of 125 cycles of increasing the temperature from −45 to 125 °C within 0.5 h.

Fabrication of wearable or skin-attachable VOC sensors is critically important in the field of real-time health monitoring and early diagnosis of diseases. This monitoring requires intrinsically deformable sensing materials that show high mechanical stability,[48,49] including high flexibility (even to a bending radius of millimeters) and high stretchability (up to a strain of 100%), while maintaining the sensing capabilities. When these requirements are satisfied, wearable VOC sensors for humans are worthy of use. However, many of the flexible and stretchable VOC sensors fabricated to date contain fragile sensing components, such as metal oxides, 2D materials, etc. Therefore, in order to overcome such problems, new sensing materials displaying high homeostasis as well as high performance are required. Our ICS was designed based on an intrinsically stretchable i-TPU sensing material, which might potentially be the core of a flexible and stretchable VOC sensor. **Figure 5**a shows the magnitude of the response of our ICS device to the 1000 ppm toluene gas when the device was bent to various extents, i.e., radii of curvature. Our device, even when

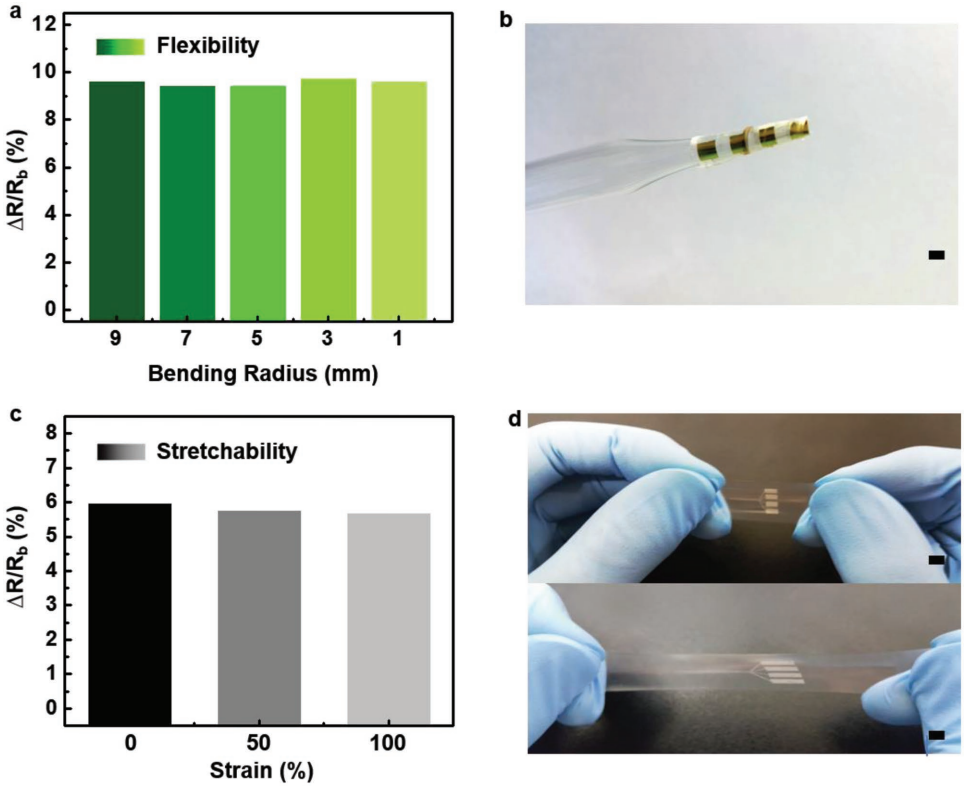

Figure 5. The ability of the ICS to sense the VOC toluene at 1000 ppm was found to be ultrastable even after the device was subjected to severe mechanical deformations. a) The resistive responses ($\Delta R/R_b$) of the ICS subjected to various degrees of bending, i.e., radii of curvature. b) Photograph of the VOC sensor on a polyethylene terephthalate substrate wrapped around a glass pipette with a radius of 1 mm. Scale bar is 2 mm. c) Response of the ICS subjected to various extents of stretching. d) Photographs of an unstrained freestanding VOC sensor (top) and one stretched by 100% (bottom). Scale bar is 2 mm.

bent quite severely to a radius of curvature of 1 mm, showed a nearly identical magnitude of response to the toluene gas as did the unbent device, i.e., no electrical degradation occurred. This result was attributed to the superior elasticity of the i-TPU electrolyte even under extreme mechanical stimuli as discussed above and shown in Figure 2. Figure 5b shows a photograph of the ICS device fabricated on a 50 μm thick polyethylene terephthalate substrate, indicating the device to be flexible enough to be wrapped around a glass pipette to a bending radius of 1 mm.

In order to eventually implement a stretchable ICS device, a freestanding deformable ICS with the i-TPU electrolyte was fabricated using only solution processes (Figure S11, Supporting Information), followed by embedding stretchable Ag nanowire electrodes into the i-TPU film via a transfer methodology. The detailed procedure is described in the Experimental Section. Figure 5c shows the magnitude of the response of our ICS device to the toluene gas when the device was stretched to various extents. Our device even when stretched by 50% or 100% showed nearly the same magnitude of response to the toluene gas as did the unstretched device. This result was attributed to the large resilience of the i-TPU electrolyte. Figure S12 in the Supporting Information shows the resistive response to various VOCs with multiple cycles (0, 100, 250, and 500) after stain of 50%. Figure 5d shows photographs of an unstrained freestanding semitransparent ICS with Ag nanowire electrodes embedded into the i-TPU electrolyte, and one stretched by 100%. Due to the functional stability of our ICS to changes in various external stimuli such as humidity, temperature, and mechanical stress, we expect that ultrastable, highly sensitive, and stretchable ICS that can effectively detect VOCs will become one of the representative platforms for skin-attachable health monitors.

In summary, we developed an ultrastable, highly sensitive, and stretchable ICS using an intrinsically stretchable i-TPU electrolyte as a sensing channel, while maintaining the unique IL properties. The VOC sensor was found to be capable of stably monitoring the five representative VOCs, specifically toluene, hexane, propanal, ethanol, and acetone. Moreover, due to the properties of the i-TPU polymer electrolyte we used, the sensor was shown to be able to robustly bear various environmental and mechanical conditions, and to still exhibit high-magnitude electrical responses to the toluene VOC. In particular, the high flexibility and stretchability of the device can allow it to adaptively interface with living tissue. We expect that VOC sensors made of the intrinsically stretchable i-TPU material that we used will be effective for the stable monitoring of VOCs, including when implemented as a human-interactive wearable device.

Supporting Information

Supporting Information is available from the Wiley Online Library or from the author.

Acknowledgements

M.L.J. and S.P. contributed equally to this work. This work was financially supported by the Center for Advanced Soft-Electronics under the Global Frontier Project (CASE-2014M3A6A5060937 and CASE-2014M3A6A5060932), the Basic Science Research Program (2015R1A2A1A05001844, 2017R1A2B4012819, and 2017R1A5A1015596), and the Global Research Development Center Program (2015K1A4A3047100) of the National Research Foundation of Korea (NRF) funded by the Ministry of Science and ICT, Korea. This work was also supported by the Ministry of Trade, Industry & Energy (MOTIE) (10051514), Korea Display Research Corporation (KDRC) support program, and the Open Innovation Program of National Nano Fabrication Center (NNFC).

Conflict of Interest

The authors declare no conflict of interest.

Keywords

intrinsically stretchable materials, ionic chemiresistor skin, solid-state polymer electrolytes, ultrastable materials, volatile organic compound sensors

Received: November 23, 2017
Revised: January 21, 2018
Published online:

[1] H. Haick, Y. Y. Broza, P. Mochalski, V. Ruzsanyi, A. Amann, *Chem. Soc. Rev.* **2014**, *43*, 1423.
[2] G. Konvalina, H. Haick, *Acc. Chem. Res.* **2014**, *47*, 66.
[3] F. Favier, E. C. Walter, M. P. Zach, T. Benter, R. M. Penner, *Science* **2001**, *293*, 2227.
[4] L.-Y. Hong, H.-N. Lin, *Beilstein J. Nanotechnol.* **2016**, *7*, 1044.
[5] C. Wang, L. Yin, L. Zhang, D. Xiang, R. Gao, *Sensors* **2010**, *10*, 2088.
[6] M. Righettoni, A. Amann, S. E. Pratsinis, *Mater. Today* **2015**, *18*, 163.
[7] R. Moos, K. Sahner, M. Fleischer, U. Guth, N. Barsan, U. Weimar, *Sensors* **2009**, *9*, 4323.
[8] H. Jin, T.-P. Huynh, H. Haick, *Nano Lett.* **2016**, *16*, 4194.
[9] F. J. Ibanez, F. P. Zamborini, *Small* **2012**, *8*, 174.
[10] G. Peng, U. Tisch, O. Adams, M. Hakim, N. Shehada, Y. Y. Broza, S. Billan, R. Abdah-Bortnyak, A. Kuten, H. Haick, *Nat. Nanotechnol.* **2009**, *4*, 669.
[11] Y. Joseph, A. Peic, X. Chen, J. Michl, T. Vossmeyer, A. Yasuda, *J. Phys. Chem. C* **2007**, *111*, 12855.
[12] E. C. Walter, K. Ng, M. P. Zach, R. M. Penner, F. Favier, *Microelectron. Eng.* **2002**, *61*, 555.
[13] E. C. Walter, R. M. Penner, *Anal. Chem.* **2002**, *74*, 1546.
[14] H.-W. Yoo, S.-Y. Cho, H.-J. Jeon, H.-T. Jung, *Anal. Chem.* **2015**, *87*, 1480.
[15] U. Lange, V. M. Mirsky, *Anal. Chem. Acta* **2011**, *687*, 105.
[16] L. K. Randeniya, P. J. Martin, A. Bendavid, J. McDonnell, *Carbon* **2011**, *49*, 5265.
[17] S. Y. Kim, S. Park, H. W. Park, D. H. Park, Y. Jeong, D. H. Kim, *Adv. Mater.* **2015**, *27*, 4178.
[18] F. Schedin, A. K. Geim, S. V. Morozov, E. W. Hill, P. Blake, M. I. Katsnelson, K. S. Novoselov, *Nat. Mater.* **2007**, *6*, 652.
[19] D. J. Late, Y.-K. Huang, B. Liu, J. Acharya, S. N. Shirodkar, J. Luo, A. Yan, D. Charles, U. V. Waghmare, V. P. Dravid, C. N. R. Rao, *ACS Nano* **2013**, *7*, 4879.
[20] J. Z. Ou, W. Ge, B. Carey, T. Daeneke, A. Rotbart, W. Shan, Y. Wang, Z. Fu, A. F. Chrimes, W. Wlodarski, S. P. Russo, Y. X. Li, K. Kalantar-zadeh, *ACS Nano* **2015**, *9*, 10313.

[21] G. Katwal, M. Paulose, I. A. Rusakova, J. E. Martinez, O. K. Varghese, *Nano Lett.* **2016**, *16*, 3014.
[22] H.-W. Ra, K.-S. Choi, J.-H. Kim, Y.-B. Hahn, Y.-H. Im, *Small* **2008**, *4*, 1105.
[23] A. Kolmakov, D. O. Klenov, Y. Lilach, S. Stemmer, M. Moskovits, *Nano Lett.* **2005**, *5*, 667.
[24] C. Wang, R. Sun, X. Li, Y. Sun, P. Sun, F. Liu, G. Lu, *Sens. Actuators, B* **2014**, *204*, 224.
[25] I.-D. Kim, A. Rothschild, B. H. Lee, D. Y. Kim, S. M. Jo, H. L. Tuller, *Nano Lett.* **2006**, *6*, 2009.
[26] S.-Y. Cho, H.-W. Yoo, J. Y. Kim, W.-B. Jung, M. L. Jin, J.-S. Kim, H.-J. Jeon, H.-T. Jung, *Nano lett.* **2016**, *16*, 4508.
[27] J. T. Robinson, F. K. Perkins, E. S. Snow, Z. Wei, P. E. Sheehan, *Nano Lett.* **2008**, *8*, 3137.
[28] A. K. Geim, K. S. Novoselov, *Nat. Mater.* **2007**, *6*, 183.
[29] J.-S. Kim, H.-W. Yoo, H. O. Choi, H.-T. Jung, *Nano Lett.* **2014**, *14*, 5941.
[30] D. Sarkar, X. Xie, J. Kang, H. Zhang, W. Liu, J. Navarrete, M. Moskovits, K. Banerjee, *Nano Lett.* **2015**, *15*, 2852.
[31] P. K. Kannan, D. J. Late, H. Morgan, C. S. Rout, *Nanoscale* **2015**, *7*, 13293.
[32] S.-Y. Cho, Y. Lee, H.-J. Koh, H. Jung, J.-S. Kim, H.-W. Yoo, J. Kim, H.-T. Jung, *Adv. Mater.* **2016**, *28*, 7020.
[33] W. Yuan, G. Shi, *J. Mater. Chem. A* **2013**, *1*, 10078.
[34] Q. H. Wang, K. Kalantar-Zadeh, A. Kis, J. N. Coleman, M. S. Strano, *Nat. Nanotechnol.* **2012**, *7*, 699.
[35] H. Li, C. Tsai, A. L. Koh, L. Cai, A. W. Contryman, A. H. Fragapane, J. Zhao, H. S. Han, H. C. Manoharan, F. Abild-Pedersen, J. K. Nørskov, X. Zheng, *Nat. Mater.* **2016**, *15*, 48.
[36] A. Rehman, X. Zeng, *RSC Adv.* **2015**, *5*, 58371.
[37] H. Niedermeyer, J. P. Hallett, I. J. Villar-Garcia, P. A. Hunt, T. Welton, *Chem. Soc. Rev.* **2012**, *41*, 7780.
[38] M. Galinski, A. Lewandowski, I. Stepniak, *Electrochim. Acta* **2006**, *51*, 5567.
[39] P. Hapiot, C. Lagrost, *Chem. Rev.* **2008**, *108*, 2238.
[40] I. Krossing, J. M. Slattery, C. Daguenet, P. J. Dyson, A. Oleinikova, H. Weingartner, *J. Am. Chem. Soc.* **2006**, *128*, 13427.
[41] R. Hayes, G. G. Warr, R. Atkin, *Chem. Rev.* **2015**, *115*, 6357.
[42] H. Ota, K. Chen, Y. Lin, D. Kiriya, H. Shiraki, Z. Yu, T.-J. Ha, A. Javey, *Nat. Commun.* **2014**, *5*, 5032.
[43] A. Chortos, G. I. Koleilat, R. Pfattner, D. Kong, P. Lin, R. Nur, T. Lei, H. Wang, N. Liu, Y.-C. Lai, M.-G. Kim, J. W. Chung, S. Lee, Z. Bao, *Adv. Mater.* **2016**, *28*, 4441.
[44] A. I. Horowitz, M. J. Panzer, *Angew. Chem., Int. Ed.* **2014**, *53*, 1.
[45] J. L. Bideau, L. Viau, A. Vioux, *Chem. Soc. Rev.* **2011**, *40*, 907.
[46] T. Sekitani, U. Zschieschang, H. Klauk, T. Someya, *Nat. Mater.* **2012**, *9*, 1016.
[47] K.-I. Jang, S. Y. Han, S. Xu, K. E. Mathewson, Y. Zhang, J.-W. Jeong, G.-T. Kim, R. C. Webb, J. W. Lee, T. J. Dawidczyk, R. H. Kim, Y. M. Song, W.-H. Yeo, S. Kim, H. Cheng, S. I. Rhee, J. Chung, B. Kim, H. U. Chung, D. Lee, Y. Yang, M. Cho, J. G. Gaspar, R. Carbonari, M. Fabiani, G. Gratton, Y. Huang, J. A. Rogers, *Nat. Commun.* **2014**, *5*, 4779.
[48] J. Y. Oh, S. Rondeau-Gagne, Y.-C. Chiu, A. Chortos, F. Lissel, G.-J. N. Wang, B. C. Schroeder, T. Kurosawa, J. Lopez, T. Katsumata, J. Xu, C. Zhu, X. Gu, W.-G. Bae, Y. Kim, L. Jin, J. W. Chung, J. B.-H. Tok, Z. Bao, *Nature* **2016**, *539*, 411.
[49] S. Savagatrup, A. D. Printz, T. F. O'Connor, A. V. Zaretski, D. J. Lipomi, *Chem. Mater.* **2014**, *26*, 3028.
[50] M. L. Jin, S. Park, Y. Lee, J. H. Lee, J. Chung, J. S. Kim, J.-S. Kim, S. Y. Kim, E. Jee, D. W. Kim, J. W. Chung, S. G. Lee, D. Choi, H.-T. Jung, D. H. Kim, *Adv. Mater.* **2017**, *29*, 1605973.
[51] S. Wagner, S. Bauer, *MRS Bulletin* **2012**, *37*, 207.
[52] J. Xu, S. Wang, G.-J. N. Wang, C. Zhu, S. Luo, L. Jin, X. Gu, S. Chen, V. R. Feig, J. W. F. To, S. Rondeau-Gagne, J. Park, B. C. Schroeder, C. Lu, J. Y. Oh, Y. Wang, Y.-H. Kim, H. Yan, R. Sinclair, D. Zhou, G. Xue, B. Murmann, C. Linder, W. Cai, J. B.-H. Tok, J. W. Chung, Z. Bao, *Science* **2017**, *355*, 59.
[53] J. Kiefer, J. Fries, A. Leipertz, *Appl. Spectrosc.* **2007**, *61*, 1306.
[54] S. Kataria, K. Singh, R. K. Singh, *J. Mater. Chem. C* **2015**, *3*, 7305.
[55] X. Chen, W. Wang, C. Jiao, *RSC Adv.* **2016**, *6*, 92276.
[56] M. Hakim, Y. Y. Broza, O. Barash, N. Peled, M. Phillips, A. Amann, H. Haick, *Chem. Rev.* **2012**, *112*, 5949.
[57] X. Zhu, H. Zhang, J. Wu, *Sens. Actuators, B* **2014**, *202*, 105.
[58] K. R. Seddon, A. Stark, M. J. Torres, *Pure Appl. Chem.* **2000**, *72*, 2275.
[59] J. Le Bideau, L. Viau, A. Vioux, *Chem. Soc. Rev.* **2011**, *40*, 907.
[60] K. Ohsawa, H. Takahashi, K. Noda, T. Kan, K. Matsumoto, I. Shimoyama, in *IEEE 24th Int. Conf. on Micro Electro Mechanical Systems*, IEEE, Cancun, Mexico **2011**, p. 525.
[61] C. Comminges, R. Barhdadi, M. Laurent, M. Troupel, *J. Chem. Eng. Data* **2006**, *51*, 680.
[62] J. Ranke, A. Othman, P. Fan, A. Müller, *Int. J. Mol. Sci.* **2009**, *10*, 1271.
[63] K. Matsunaga, K. Sato, M. Tajima, Y. Yoshida, *Polymer* **2005**, *37*, 413.